

Nuclear model effects in Charged Current neutrino–nucleus quasielastic scattering

C. Maierón, M.C. Martínez and J.A. Caballero

Departamento de Física Atómica, Molecular y Nuclear

Universidad de Sevilla, Apdo. 1065, E-41080 Sevilla, SPAIN

J.M. Udías

Departamento de Física Atómica, Molecular y Nuclear

Universidad Complutense de Madrid, E-28040 Madrid, SPAIN

(February 20, 2019)

Abstract

The quasielastic scattering of muon neutrinos on oxygen 16 and carbon 12 targets is studied for neutrino energies between 200 MeV and 1 GeV, using the relativistic Fermi gas and a relativistic shell model. Final state interactions are included within the distorted wave impulse approximation. The different models are then employed to compute the inclusive charged-current quasielastic cross section for $\nu_\mu - {}^{12}C$ scattering in the kinematical conditions of the LSND experiment at Los Alamos.

13.15.+g; 25.30.Pt; 24.10.Jv

Typeset using REVTEX

I. INTRODUCTION

In the past decades neutrino scattering on complex nuclei has received considerable attention, both experimentally and from the theoretical point of view. Besides their interest as a probe of nuclear and, at higher energies, nucleonic structure, these processes are important for the detection of neutrinos both from astrophysical sources and in Earth-based neutrino oscillation experiments. In fact, neutrino detectors, such as liquid-scintillator or water Čerenkov detectors, usually contain carbon or oxygen nuclei, and for a proper interpretation of the experimental results the description of the ν -nucleus interaction must be accurate.

The interest towards these processes has further increased in the past few years, after the indications of neutrino oscillations observed by the Super-Kamiokande collaboration [1,2]. Several experiments are now planned or under construction (see, for example, [3–5] and references therein), aimed at determining the neutrino oscillation parameters with high precision. In these measurements the data analysis will be more sensitive to sources of systematic errors, among them nuclear structure and final state interaction effects, motivating a “new round” of theoretical calculations [6].

At intermediate neutrino energies, ranging from about a hundred MeV to a few GeV, ν -nucleus quasielastic scattering has been studied within several approaches. The simplest mean field model is the Fermi gas, which has been employed both in non-relativistic and relativistic versions [7–9]. Extensions of this model have been considered by Kim and collaborators [10,11], within a relativistic meson nucleon model, including particle-hole and delta-hole excitations and momentum dependent single nucleon self-energies. In agreement with a previous non-relativistic calculation of Singh and Oset [12], their results showed random phase approximation (RPA) corrections to be relevant only at low momentum transfers. More specific calculations of RPA effects on the measurements of atmospheric neutrinos have also been done [13–15], leading to the conclusion that although the calculated effects were not enough to explain the observed anomaly in the ν_e/ν_μ ratios of atmospheric neutrino fluxes, more accurate theoretical estimates were needed for future and precise data analyses. Recently Bleve and collaborators [16,17] have drawn the attention towards final state interaction effects showing that, within a phenomenological convolution model applied to the relativistic Fermi gas, nucleon re-scattering can produce a reduction of the quasielastic cross section as large as 15% at the relatively high energy $E_\nu = 1$ GeV.

At lower neutrino energies, inclusive neutrino processes on ^{12}C have been measured by the LSND collaboration at Los Alamos [18–20]. Their first measurements of the inclusive cross section for the process $^{12}C(\nu_\mu, \mu^-)X$, averaged over the Los Alamos ν_μ Decay-in-Flight beam, provided a value which was more than factor two smaller than a previous RPA theoretical prediction [18,21]. This result stimulated new and more accurate theoretical calculations, which were carried on by several groups, both within the RPA [22–26] and using the shell model to describe the mother and daughter nuclear systems [26–29]. Presently the discrepancy between the theory and the most recent experimental findings [19,20] has been slightly reduced, down to about 20–25% for shell model calculations and 40% for RPA approaches [26] (we observe however that a recent projected RPA calculation [30] obtains a result which is about only 20% higher than the experiment). Calculations that take into account meson exchange current contributions to this process [31] show that they produce

a reduction of the cross-section of the order of 6%, not enough to drive the theory in agreement with experiment. The only prediction in good agreement with the experiment is the calculation by Mintz and Pourkaviani [32], based on a so called “elementary particle model”, but doubts have been expressed on whether this model can be extrapolated at the low neutrino energies available at Los Alamos [33].

On the contrary, in general all theoretical models [22,24–26,28] reproduce reasonably well the cross sections for the related processes of exclusive transition to the ^{12}N ground state, $^{12}C(\nu_\mu, \mu^-)^{12}N_{g.s.}$, of muon capture on ^{12}C [34] as well as both inclusive and exclusive cross sections for the scattering on ^{12}C of electron neutrinos produced by muon-Decay-at-rest, measured by the LSND and the KARMEN collaborations [35,36].

In this contribution we consider the quasielastic scattering of muon neutrinos on ^{16}O and ^{12}C , described within the impulse approximation (IA). We first study the modification, with respect to the relativistic Fermi gas description (RFG), produced by using a more realistic relativistic shell model (RSM) and then, within the RSM approach, we evaluate the effects of final state interactions (FSI) between the emitted nucleon and the residual system, by using, for the outgoing nucleon, distorted waves already successfully employed in the calculation of (exclusive) electron scattering processes [37–39].

We initially consider fixed incident neutrino energies, in the range 200 MeV – 1 GeV, where the quasielastic nucleon knockout is expected to be the dominant contribution to the ν -nucleus scattering process. At higher energies inelastic contributions become increasingly dominant in the inclusive process, while at much lower energies the excitation of nuclear resonances should be included in the calculation. We will show that, while within the Plane Wave Impulse Approximation (PWIA) nuclear model effects are reduced with increasing neutrino energy, becoming almost negligible at $E_\nu = 1$ GeV, FSI effects do not disappear as rapidly, remaining sizeable even at the highest energy values we have considered.

We then employ our models to compute the inclusive $\nu_\mu - ^{12}C$ charged current quasielastic scattering cross section in the LSND kinematical conditions, showing that FSI effects can produce a reduction of at least 20%. However, in agreement with the calculations of other groups within different approaches, our results are larger than the experimental value.

Since the muon neutrino energies available at Los Alamos range between muon-threshold (about 120 MeV) and 300 MeV, quasielastic scattering may not be the only relevant contribution to the process we are considering. However, the inclusion of FSI effects within the distorted wave impulse approximation (DWIA), and in particular what we call relativistic mean field approach, takes into account the contribution to the integrated cross section of the first excited states of ^{12}N , which are known to decay immediately by proton emission. We thus think that, although non completely realistic, our calculation may anyway provide useful indications about the role of FSI in this interesting process, and may shed light on the discrepancy of the theoretical results among themselves and with the experiment.

II. FORMALISM

Let us consider the charged current (CC) quasielastic scattering of (muon) neutrinos on a nuclear target, which at lowest order in the electroweak interaction is described by the exchange of one charged vector boson.

We describe this process within the impulse approximation, assuming that the incident neutrino interacts with only one nucleon (neutron), which is then emitted, while the remaining ($A-1$) nucleons in the target are spectators. The nuclear current is assumed to be the sum of single nucleon currents and the states of the target and residual nuclei to be adequately described by an independent particle model wave function. In particular, we use relativistic shell model wave functions, which have been widely tested in studies of exclusive quasielastic electron–nucleus scattering [37–39].

As a reference for evaluating the impact of the different nuclear effects, we also calculate neutrino cross sections within the relativistic Fermi gas model. RFG cross sections have been already calculated and presented in several works [7,9,40], but, since the inclusion of binding energy effects can generate some ambiguity, in the Appendix we report the explicit expressions we have used in our numerical calculations. We notice however that the numerical differences with respect to other authors for the results including binding energy effects are limited to a few percent.

The formalism we employ for the RSM case has been extensively described elsewhere, both for electron scattering processes [37–39] and for neutrino scattering [41], thus we limit our description to those aspects which are of more relevance for the discussion that follows. Within the IA, the process we are interested in is described in fig. 1, which defines our conventions for the kinematical variables.

In our numerical calculations we consider ^{16}O and ^{12}C targets, whose ground states we describe as closed shell configurations, the occupied shells being $s_{1/2}$, $p_{3/2}$ and $p_{1/2}$ for oxygen and $s_{1/2}$ and $p_{3/2}$ for carbon. For the removal of a nucleon from a closed shell of angular momentum j , the cross section corresponding to the diagram in fig. 1 has the following general form ¹:

$$\frac{d^6\sigma}{d^3k'd^3p_N} = \int \delta^{(4)}(q + p_A - p_{A-1} - p_N) \frac{G_F^2}{(2\pi)^5} \frac{(2j+1)}{8E_\nu E_\mu} \overline{\sum} |\bar{u}(k')\gamma^\alpha (1 + \gamma_5) u(k) J_\alpha(\mathbf{q})|^2 d^3p_{A-1}, \quad (1)$$

where $G_F = 1.166 \times 10^5 \text{ GeV}^{-2}$ [42] is the Fermi constant and $\overline{\sum}$ indicates the average/sum over the initial/final spins. We then sum over the occupied shells and integrate over the emitted nucleon and over the direction of the outgoing muon in order to get the inclusive cross sections $\frac{d\sigma}{dT_\mu}$, and the integrated inclusive cross section $\sigma = \int \frac{d\sigma}{dT_\mu} dT_\mu$, T_μ being the outgoing lepton kinetic energy.

The main ingredient in eq. (1) is the single nucleon current matrix element,

$$J_\alpha(\mathbf{q}) = \sqrt{V} \int d^3r e^{i\mathbf{q}\cdot\mathbf{r}} \bar{\psi}_{s_N}(\mathbf{p}_N, \mathbf{r}) \hat{\Gamma}_\alpha \psi_B^{jm}(\mathbf{r}), \quad (2)$$

where $\psi_B^{jm}(\mathbf{r})$ and $\psi_{s_N}(\mathbf{p}_N, \mathbf{r})$ are the wave functions for the initial (bound) nucleon and for the emitted nucleon, respectively, and $\hat{\Gamma}_\alpha$ is the single nucleon weak CC current operator. For the latter we assume the free, on mass shell, nucleon expression:

¹Here $\gamma_5 = -i\gamma^0\gamma^1\gamma^2\gamma^3$ and Dirac spinors are normalized according to $u(k)^\dagger u(k) = 2k_0$.

$$\hat{\Gamma}_\alpha = |V_{ud}| \left[F_V \gamma_\alpha + F_M \frac{i}{2m_N} \sigma_{\alpha\beta} q^\beta + F_A \gamma_\alpha \gamma_5 - F_P q_\alpha \gamma_5 \right], \quad (3)$$

where $F_{V,M}$ are the CC single nucleon Pauli and Dirac form factors, F_A and F_P are the axial and the induced pseudoscalar form factor, respectively, and $|V_{ud}| = 0.975$ [42] is the ud Cabibbo–Kobayashi–Maskawa matrix element. In the following our focus will be on nuclear structure effects, but a few comments on the impact of single nucleon form factors on ν –nucleus cross section will be made when presenting numerical results.

In eq. (2) the bound nucleon wave functions $\psi_B^{jm}(\mathbf{r})$ are the self-consistent (Hartree) solutions of a Dirac equation, derived, within a Relativistic Mean Field approach, from a Lagrangian containing σ , ω and ρ mesons [43]. As the single-particle binding energies determine the threshold of the cross section for every shell, in the numerical calculations, we have used the experimental values corresponding to the binding energies of the different shells.

For the outgoing nucleon wave functions the simplest choice is to use plane wave spinors, i.e., no interaction is considered between the ejected nucleon and the residual nucleus (PWIA). For a more realistic description, FSI effects should be taken into account. In our formalism this is done by using distorted waves which, in analogy with several studies of $(e, e'N)$ reactions, are given as solutions of a Dirac equation containing a phenomenological relativistic optical potential (hereafter referred to as ROP), consisting of a real part, which describes the rescattering of the ejected nucleon and of an imaginary part, that accounts for the absorption of it into unobserved channels. The parameters of the ROP are fitted to elastic nucleon-nucleus scattering data in an extensive range of proton energies and mass number nuclei. In this work we use the ROP corresponding to the EDAD-1 single-nucleon parameterization presented in ref. [44]. As shown in [37–39], the use of this phenomenological ROP leads to an excellent agreement between theoretical calculations and data for exclusive $(e, e'N)$ observables; however some caution should be taken in extending the conclusions drawn from the analysis of exclusive reactions to inclusive ones. In the latter, since all final channels are included, the presence of the imaginary term in the optical potential may lead to an overestimation of FSI effects. Hence in our calculation we set to zero the imaginary part; however, in some of the figures that follow we also show the results corresponding to the global ROP model, which can provide an extreme limit of the role of FSI.

Finally, for small energy transfer one may also use distorted waves which are obtained as the solutions in the continuum of the same Dirac equation used to describe the initial bound nucleon. In the following we will refer to this approach as relativistic mean field (RMF). We believe that, together, the RMF and ROP results indicate a reasonable “band” where the FSI effects should lie.

A different type of “final state interaction” arises from the distortion of the outgoing muon wave function in the Coulomb field of the recoiling nucleus ². A rigorous description of this correction is somewhat complicated (see for instance refs. [37,45]), as it would require the use, for the outgoing lepton, of distorted waves which are eigenfunctions of the nuclear

²The Coulomb distortion of the emitted proton is included in the ROP and RMF descriptions of FSI.

Coulomb field; however its main effects can be described within approximate approaches. At low outgoing lepton kinetic energies ($T_\mu \lesssim 10$ MeV) Coulomb distortion can be accounted for by multiplying the differential cross section ($d\sigma/dT_\mu$) by the correction factor [13,32,46]

$$F(Z, E_\mu) = \frac{2\pi\eta}{1 - e^{-2\pi\eta}}, \quad (4)$$

where $\eta = \pm(Z\alpha)E_\mu/|\mathbf{k}'|$ (α being the fine structure constant) and the plus and minus signs are used for leptons and antileptons, respectively.

For higher energy leptons this approximation is not adequate. For this reason, and in analogy with studies of Coulomb distortion effects in electron–nucleus quasielastic scattering [47,48], we use the so called “effective momentum approximation”, which prescribes to substitute the plane wave describing the outgoing lepton with the function $\frac{|\mathbf{k}'_{eff}|}{|\mathbf{k}'|} e^{i\mathbf{k}'_{eff} \cdot \mathbf{r}}$,

where the effective momentum is given by $\mathbf{k}'_{eff} = \mathbf{k}' \pm V_c \frac{\mathbf{k}'}{|\mathbf{k}'|}$ (again the plus/minus sign refers to leptons/antileptons) and V_c is the nuclear Coulomb potential which, for a uniformly charged sphere of radius $R \simeq 1.2A^{\frac{1}{3}}$ fm, is given by $V_c = 3Z\alpha/2R$; however, the comparison with an exact calculation for electron scattering [37], has shown that this value may overestimate the Coulomb effects ($\sim 30\%$).

III. RESULTS

In this section we present the results of our calculations of the CC cross sections for the quasielastic scattering of muon neutrinos on oxygen and carbon nuclei.

In general, for the comparison with experimental measurements, ν –nucleus cross sections require an additional integration over the incident neutrino energy, weighted with the appropriate neutrino spectrum. This procedure depends on the experimental conditions under consideration and, moreover, it introduces additional uncertainties in the calculations.

Therefore we first make a general study of nuclear model effects, by fixing the incident neutrino energy to three “typical” values, 200 MeV, 500 MeV, and 1 GeV, in a range where quasielastic scattering is expected to represent the main contribution to the inclusive ν –nucleus process. Then we will use our model to compute the flux-averaged cross section for $\nu_\mu - {}^{12}C$ quasielastic scattering in the kinematic conditions of the LSND experiment at Los Alamos [18–20] and compare our results with the corresponding experimental value for the process ${}^{12}C(\nu_\mu, \mu^-)X$.

A. Fixed incident neutrino energy

For better clarity, in studying the impact of nuclear structure on neutrino–nucleus cross section we take two steps: we first study the effects of using different nuclear models within the PWIA and subsequently we analyze the effects of FSI.

The curves we show in this subsection are calculated for the scattering of muon neutrinos on oxygen 16, but very similar results are obtained when considering a carbon 12 target. In

the figures we present, we do not explicitly include the effects of the outgoing muon Coulomb distortion. They are relevant only at low neutrino energies: for the case $E_\nu = 200$ MeV we find that Coulomb distortion produces an enhancement of the cross section of less than 10%, while at higher energy the corrections are below $1 \div 2\%$.

The nuclear model dependence in PWIA is illustrated in fig. 2, which shows the differential cross section ($d\sigma/dT_\mu$) as a function of the outgoing muon kinetic energy, for $E_\nu = 200$ MeV (upper panel), 500 MeV (middle) and 1 GeV (lower panel). Here the results obtained with the RFG, without (dot-dashed line) and with (dotted) binding energy, are compared with the RSM (solid). Let us focus on the case $E_\nu = 200$ MeV, where nuclear structure effects are more evident. As expected, we see that including the binding energy results both in a reduction and in a shift of the RFG cross section towards lower T_μ values. When using the RSM, we observe also a change in the shape of the cross section, due to the different momentum distributions of the single nucleon shells contributing to the process. Since the various shells have different binding energies, the corresponding contributions to the cross section go to zero at different values of T_μ , namely $\bar{T}_\mu \simeq E_\nu - m_\mu - e_B^{shell}$, and this gives rise to the structure of ($d\sigma/dT_\mu$) observed at large T_μ .

When the incident neutrino energy increases, the model dependence becomes less relevant, almost disappearing at $E_\nu = 1$ GeV.

On the other hand, the behavior of FSI effects is quite different, as illustrated in fig. 3. Here the results obtained with the RSM in PWIA (solid) are compared with the cases where FSI are described within the RMF (dashed) and the purely real ROP (dotted) approaches, previously described. The result corresponding to the global ROP, i.e., including an imaginary term, is also indicated for reference (dot-dashed). Note that the use of real potentials (RMF and real ROP) for describing the final nucleon states leads to the resonant structure observed for relatively high T_μ (that is, small energy transfer ω).

We observe that FSI effects, both within the RMF and ROP approaches, produce a reduction of the cross section, particularly important in the case of the complex ROP model due to the absorption introduced by the imaginary term. In the region close to the maximum, this reduction, which, as already mentioned, may be an overestimation of the FSI effects, is about 60% for $E_\nu = 200$ MeV and 50% for $E_\nu = 500$ MeV and $E_\nu = 1$ GeV. For the RMF and real ROP, the reduction, similar in both cases, is about $30 \div 40\%$ for $E_\nu = 200$ MeV and 20% for the other energy values.

Finally, nuclear model effects on integrated cross sections are studied in fig. 4, where the cross section $\sigma(E_\nu)$ is plotted as a function of the incident neutrino energy. Again we see that within the PWIA the discrepancy between different nuclear models is relatively small and decreases with increasing neutrino energy. On the contrary FSI effects remain sizeable even at large E_ν . Here, the contributions coming from the RMF and ROP resonances have been included in the calculation, in order to respect the completeness of the set of final states predicted by the model. These contributions are important at $E_\nu = 200$ MeV, where they amount to about 10% of the integrated cross section, while at higher energies these effects are about 2% (500 MeV) and 1% (1 GeV). As in the previous figure, the role played by the imaginary term in the ROP leads to a very significant reduction ($\sim 50\%$) of the integrated cross section. On the contrary the results for the RMF and real ROP models, which do not differ appreciably, show a much smaller reduction.

Up to now we have discussed the sensitivity of ν -nucleus cross section to different nuclear

models, which is the main focus of this paper. However, ν -nucleus quasielastic cross section, can be sensitive also to the single nucleon structure, which enters the cross section through the CC current in eq. (3). In particular the effects of the axial form factor F_A , especially for relatively high values of the four-momentum transfer Q^2 , are known to be relevant. To test this sensitivity we have assumed the usual dipole parameterization $F_A = \frac{g_A}{(1 + Q^2/M_A^2)}$ with $g_A = 1.267$ [42], letting the axial cutoff mass vary in the range $M_A = 1.026 \pm 0.021$ GeV, which corresponds to the world average as measured in neutrino scattering experiments [49]. In agreement with previous findings we observe that the dependence on the axial form factor increases at large neutrino energy, ranging, for the values of M_A we have considered, between $\pm 0.7\%$ at $E_\nu = 200$ MeV and $\pm 3\%$ at $E_\nu = 1$ GeV. We do not observe any significant dependence on other form factors.

B. LSND kinematical conditions

Let us now turn to the kinematical conditions of the LSND experiment at Los Alamos, where the inclusive $^{12}(\nu_\mu, \mu^-)X$ cross section, including contributions from all accessible final channels, was measured using a pion-Decay-in-Flight ν_μ beam, with energies ranging from zero to 300 MeV, and a large liquid scintillator detector [18–20].

At these low energies, processes different from the quasielastic nucleon knockout are expected to contribute to the inclusive cross section: besides the transition to the ^{12}N ground state, for which the measured exclusive cross section is about 5% of the total value, transitions to the first $^{12}N^*$ excited states, which immediately decay by proton emission, should be considered. In our approach these contributions are simulated through the inclusion of FSI effects, within the frameworks of the RMF and the purely real ROP.

In order to compare our results with the experimental measurements we calculate flux-averaged cross sections

$$\langle \frac{d\sigma}{dT_\mu} \rangle = \frac{\int_{E_{min}}^{E_{max}} dE_\nu \phi(E_\nu) \frac{d\sigma}{dT_\mu}(E_\nu)}{\int_{E_{min}}^{E_{max}} dE_\nu \phi(E_\nu)}, \quad (5)$$

$$\langle \sigma \rangle = \int dT_\mu \langle \frac{d\sigma}{dT_\mu} \rangle \quad (6)$$

using the 1994 Los Alamos neutrino spectrum $\phi(E_\nu)$ [18], which was used in previous theoretical calculations, and the limits $E_{min} = 123.1$ MeV and $E_{max} = 300$ MeV. As stated in [20] the final flux shape, averaged over the years, is practically the same as the one calculated for 1994, although we notice that using the neutrino spectrum taken from fig. 2 of ref. [20] the results we obtain are about a 20–25% larger than the ones we present here. We observe that, in the RFG calculations, our threshold for muon production would be slightly smaller than the above value, while, for the results presented in this subsection, the binding energies of the initial states for the RSM are chosen to reproduce the experimental threshold $E_{min} = 123.1$ MeV.

Since the flux averaging procedure can introduce uncertainties in the comparison with other theoretical results, and to better illustrate the ingredients of our calculation, we also

consider a fixed value of the incident neutrino energy, namely $E_\nu = 156$ MeV, corresponding to the average energy of the Los Alamos beam. This case is illustrated in fig. 5, where the effects of different nuclear models within the PWIA and including FSI evaluated within the RMF and real ROP approaches are shown. These results are similar to those obtained in the lowest energy case of the previous subsection: in PWIA using the RSM model (solid line) essentially reduces the T_μ interval where the cross section is different from zero, while FSI diminish the cross section, this reduction being similar for the two approaches considered. We observe that the main contribution to $d\sigma/dT_\mu$ in the RSM comes from the removal of a nucleon from the $p_{3/2}$ shell, while the $s_{1/2}$ shell only contributes at small T_μ (high ω), due to the relatively large value (42.3 MeV) of the corresponding binding energy.

In fig. 6 we show the observed [19] and calculated distribution of events versus the muon kinetic energy. The theoretical distributions have been normalized to the data for the flux-averaged cross section, and the same bin in energy as for the experimental data (5 MeV) has been employed. The shape and position of the maximum of the experimental distribution is approximately reproduced by the three calculations and overall the RSM-PWIA predictions seems to fit the data slightly better.

The values we obtain for the flux-averaged integrated cross section are listed in table I. Within PWIA we see that the difference between the RSM and the RFG is moderate, once binding energy effects are included in the RFG. On the other hand, within the RSM approach, FSI produce a reduction of the cross section, of the order of 18% (RMF) and 26% (real ROP), which brings the theoretical prediction closer to the experimental result. However, and in general agreement with other theoretical predictions, this reduction is not enough to explain the experimental data, which remain below our results. Although not shown, it is interesting to point out that the use of the global complex ROP leads to a very significant reduction of the cross section, of the order of 50%, compared with the PWIA result.

The results shown in table I do not include the Coulomb distortion of the outgoing muon. When evaluated within the effective impulse approximation, these effects produce an enhancement of the cross section between 6% and 10%, the upper limit being obtained with a nuclear Coulomb field V_c for a uniform spherical charge and the lower limit corresponding to a constant $V_c = 2.5$ MeV, as suggested by an analysis of electron scattering processes [37]. We notice that the correction factor of eq. (4), which has often been used in the literature for the kinematical conditions we are now considering, would produce an increase of the cross sections of about 25%.

With this in mind we can conclude that our RMF and ROP approaches give predictions which are a factor ≈ 2 larger than the measured central value.

Finally let us consider the dependence of the cross sections on the single nucleon form factors. At the Los Alamos kinematics the values of the four-momentum transfer are rather low ($Q^2 \simeq 0 \div 0.2$ (GeV/c) 2) and thus the choice of different form factors parameterizations, in particular for F_A , does not introduce significant uncertainties in the results. At such low energies one may expect, however, some effects arising from the induced pseudoscalar form factor, which is often neglected in the calculations, since at intermediate and high energies its contribution is irrelevant. In order to evaluate these effects we have assumed the parameterization $F_P = -\frac{2m_N}{Q^2 + m_\pi^2} F_A$, based on the PCAC hypothesis and the pion

pole dominance, which, at the low Q^2 we are considering, almost coincides with the chiral perturbation theory result of ref. [49]. Since very little is known about F_P , we have calculated the flux-averaged integrated neutrino cross section using $0.5F_P$ and $1.5F_P$, obtaining a 2% enhancement and a 1 % reduction, respectively, thus confirming that even in this kinematical regime the uncertainty associated to the pseudoscalar form factor is small.

IV. SUMMARY AND CONCLUSIONS

We have employed a relativistic shell model to study nuclear model effects in ν_μ CC quasielastic scattering on carbon and oxygen targets, in the intermediate neutrino energy region $E_\nu = 200\text{--}1000$ MeV. We have observed that within the PWIA nuclear model effects practically disappear at high energies, while the reduction of the cross sections due to FSI remains sizeable, being, for example, at least 14% at $E_\nu = 1$ GeV. We thus conclude that these effects should be carefully considered in neutrino experiments which use carbon or oxygen based detectors. We have then applied our model to the calculation of the inclusive $\nu_\mu - {}^{12}C$ cross section at the kinematics of the LSND experiment, observing that FSI produce a significant reduction, with respect to PWIA, of the cross section, although it is still larger than the experimental data, in analogy with previous analyses.

ACKNOWLEDGEMENTS

This work was partially supported by funds provided by DGI (Spain) and FEDER funds, under Contracts Nos BFM2002-03315, FPA2002-04181-C04-04 and BFM2000-0600 and by the Junta de Andalucía. C.M. acknowledges financial support from MEC (Spain) for a postdoctoral stay at University of Sevilla (ref. SB2000-0427). M.C.M. acknowledges support from a fellowship from the Fundación Cámara (University of Sevilla).

APPENDIX

The explicit formula we have used for calculating the cross section ($d\sigma/dT_\mu$) in the relativistic Fermi gas model, including a possible binding energy e_B , is the following

$$\begin{aligned} \frac{d\sigma}{dT_\mu} = & \frac{3N}{8\pi k_F^3} \frac{G_F^2 |V_{ud}|^2}{(2\pi)^2} \frac{|\mathbf{k}'|}{E_\nu} \int d\Omega_\mu \int \frac{d^3 p_N}{E_N} \int \frac{d^3 p}{E} \theta(|\mathbf{p}_N| - k_F) \theta(k_F - |\mathbf{p}|) \\ & \times \delta^3(\mathbf{p}_N - \mathbf{q} - \mathbf{p}) \delta(E_N - \omega - E + e_B) \left[W_V F_V^2 + W_M F_M^2 + W_{VM} F_V F_M \right. \\ & \left. + W_A F_A^2 + W_P F_P^2 + W_{AP} F_A F_P + W_{AM} F_A F_M + W_{AV} F_A F_V \right] \end{aligned} \quad (7)$$

where $E = \sqrt{\mathbf{p}^2 + m_N^2}$, N is the number of neutrons in the target, $F_{V,M,A,P}$ are the single nucleon CC form factors introduced in eq. (3) and

$$W_V = 2 \left[(k \cdot p)(k' \cdot p_N) + (k \cdot p_N)(k' \cdot p) - (k \cdot k')m_N^2 \right] \quad (8)$$

$$W_M = \frac{(k \cdot k')}{m_N^2} \left[(k \cdot p)(k \cdot p_N) + (k' \cdot p)(k' \cdot p_N) + (k \cdot k')m_N^2 \right] \\ - \frac{m_\mu^2}{4m_N^2} \left[3(k \cdot k')m_N^2 + 4(k \cdot p)(k \cdot p_N) + (k \cdot k')(p \cdot p_N) \right] \quad (9)$$

$$W_A = 2 \left[(k \cdot p)(k' \cdot p_N) + (k \cdot p_N)(k' \cdot p) + (k \cdot k')m_N^2 \right] \quad (10)$$

$$W_P = m_\mu^2(k \cdot k') \left[(p \cdot p_N) - m_N^2 \right] \quad (11)$$

$$W_{VM} = 2(k \cdot k') (p - p_N) \cdot (k - k') + m_\mu^2 (k \cdot p_N - k \cdot p) \quad (12)$$

$$W_{AP} = 2m_N m_\mu^2(k \cdot p - k \cdot p_N) \quad (13)$$

$$W_{AV} = 4 \left[(k \cdot p)(k' \cdot p_N) - (k \cdot p_N)(k' \cdot p) \right] \quad (14)$$

$$W_{AM} = 2 \left[k \cdot p_N + k \cdot p + k' \cdot p_N + k' \cdot p \right] (k \cdot k') \\ - 2m_\mu^2 (k \cdot p_N + k \cdot p) . \quad (15)$$

In order to maintain the same integration order as in the RSM calculations, we have used the delta over the three-momentum to integrate over d^3p by fixing $\mathbf{p} = \mathbf{q} + \mathbf{p}_N$ and the energy conserving delta function to integrate over $\cos \theta_N = \frac{\mathbf{p}_N \cdot \mathbf{q}}{|\mathbf{p}_N| |\mathbf{q}|}$ by setting

$$\cos \theta_N = \frac{\mathbf{q}^2 - \omega^2 + 2\omega E_N - e_B (e_B + 2E_N - 2\omega)}{2|\mathbf{p}_N| |\mathbf{q}|} . \quad (16)$$

The integrations over the azimuthal angles of the vectors \mathbf{p}_N and \mathbf{k}' are then done analytically, while we integrate numerically over E_N and $\cos \theta_\mu = \frac{\mathbf{k}' \cdot \mathbf{q}}{|\mathbf{k}'| |\mathbf{q}|}$.

REFERENCES

- [1] Y. Fukuda *et al.* [Super-Kamiokande Collaboration], Phys. Rev. Lett. **81**, 1562 (1998).
- [2] for a review of these and of more recent results, see C. K. Jung, C. McGrew, T. Kajita and T. Mann, Ann. Rev. Nucl. Part. Sci. **51**, 451 (2001); E. T. Kearns, Frascati Phys. Ser. **28**, 413 (2002) [arXiv:hep-ex/0210019].
- [3] A. De Santo, Int. J. Mod. Phys. A **16**, 4085 (2001).
- [4] R. Stefanski [MiniBOONE Collaboration], Nucl. Phys. Proc. Suppl. **110**, 420 (2002).
- [5] R. Saakian [MINOS Collaboration], Nucl. Phys. Proc. Suppl. **111**, 169 (2002).
- [6] see “Neutrino Nucleus Interactions In The Few GeV Region”. Proceedings, 1st International Workshop, Nuint01, Tsukuba, Japan, December 13-16, 2001.
- [7] R. A. Smith and E. J. Moniz, Nucl. Phys. B **43**, 605 (1972) [Erratum-ibid. B **101**, 547 (1975)].
- [8] T. K. Gaisser and J. S. O’Connell, Phys. Rev. D **34**, 822 (1986).
- [9] T. Kuramoto, M. Fukugita, Y. Kohyama and K. Kubodera, Nucl. Phys. A **512**, 711 (1990).
- [10] H. c. Kim, J. Piekarewicz and C. J. Horowitz, Phys. Rev. C **51**, 2739 (1995).
- [11] H. c. Kim, S. Schramm and C. J. Horowitz, Phys. Rev. C **53**, 2468 (1996).
- [12] S. K. Singh and E. Oset, Phys. Rev. C **48**, 1246 (1993).
- [13] J. Engel, E. Kolbe, K. Langanke and P. Vogel, Phys. Rev. D **48**, 3048 (1993).
- [14] H. c. Kim, S. Schramm and C. J. Horowitz, Phys. Rev. C **53**, 3131 (1996).
- [15] J. Marteau, J. Delorme and M. Ericson, Nucl. Instrum. Meth. A **451**, 76 (2000).
- [16] C. Bleve, G. Cò, I. De Mitri, P. Bernardini, G. Mancarella, D. Martello and A. Surdo, Astropart. Phys. **16**, 145 (2001).
- [17] G. Cò, C. Bleve, I. De Mitri and D. Martello, Nucl. Phys. Proc. Suppl. **112**, 210 (2002).
- [18] M. Albert *et al.* [LSND Collaboration], Phys. Rev. C **51**, 1065 (1995).
- [19] C. Athanassopoulos *et al.* [LSND Collaboration], Phys. Rev. C **56**, 2806 (1997).
- [20] L. B. Auerbach *et al.* [LSND Collaboration], Phys. Rev. C **66**, 015501 (2002).
- [21] E. Kolbe, K. Langanke and S. Krewald, Phys. Rev. C **49**, 1122 (1994).
- [22] E. Kolbe, F. K. Thielemann, K. Langanke and P. Vogel, Phys. Rev. C **52**, 3437 (1995).
- [23] H. c. Kim, J. Piekarewicz and C. J. Horowitz, “Relativistic treatment of the charged current reaction $^{12}C(\nu_\mu, \mu^-)$ near threshold”, arXiv:nucl-th/9502041.
- [24] S. K. Singh, N. C. Mukhopadhyay and E. Oset, Phys. Rev. C **57**, 2687 (1998).
- [25] N. Jachowicz, K. Heyde, J. Ryckebusch and S. Rombouts, Phys. Rev. C **65**, 025501 (2002).
- [26] C. Volpe, N. Auerbach, G. Colò, T. Suzuki and N. Van Giai, Phys. Rev. C **62**, 015501 (2000) 015501.
- [27] N. Auerbach, N. Van Giai and O. K. Vorov, Phys. Rev. C **56**, 2368 (1997).
- [28] A. C. Hayes and I. S. Towner, Phys. Rev. C **61**, 044603 (2000).
- [29] N. Auerbach and B. A. Brown, Phys. Rev. C **65**, 024322 (2002).
- [30] F. Krmpotic, A. Mariano and A. Samana, Phys. Lett. B **541**, 298 (2002).
- [31] Y. Umino, J. M. Udías and P. J. Mulders, Phys. Rev. Lett. **74**, 4993 (1995); Y. Umino and J. M. Udías, Phys. Rev. C **52**, 3399 (1995).
- [32] S. L. Mintz and M. Pourkaviani, Nucl. Phys. A **594**, 346 (1995).
- [33] E. Kolbe, K. Langanke and P. Vogel, Nucl. Phys. A **613**, 382 (1997).

- [34] T. Suzuki, D. F. Measday and J. P. Roalsvig, Phys. Rev. C **35**, 2212 (1987).
- [35] L. B. Auerbach *et al.* [LSND Collaboration], Phys. Rev. C **64**, 065501 (2001).
- [36] B. E. Bodmann *et al.* [KARMEN Collaboration], Phys. Lett. B **332**, 251 (1994).
- [37] J.M. Udías, P. Sarriguren, E. Moya de Guerra, E. Garrido and J.A. Caballero, Phys. Rev. C **48**, 2731 (1993); Phys. Rev. C **51**, 3246 (1995).
- [38] J.M. Udías, P. Sarriguren, E. Moya de Guerra and J.A. Caballero, Phys. Rev. C **53**, R1488 (1996).
- [39] J.M. Udías, J.A. Caballero, E. Moya de Guerra, J.E. Amaro and T.W. Donnelly, Phys. Rev. Lett. **83**, 5451 (1999); J.M. Udías, J.A. Caballero, E. Moya de Guerra, J.R. Vignote and A. Escuderos, Phys. Rev. C **64**, 024614-1 (2001).
- [40] C. J. Horowitz, H. c. Kim, D. P. Murdock and S. Pollock, Phys. Rev. C **48**, 3078 (1993).
- [41] W. M. Alberico *et al.*, Nucl. Phys. A **623**, 471 (1997); Phys. Lett. B **438**, 9 (1998).
- [42] K. Hagiwara *et al.* [Particle Data Group Collaboration], Phys. Rev. D **66**, 010001 (2002).
- [43] C.J. Horowitz and B.D. Serot, Nucl. Phys. A **368**, 503 (1981); Phys. Lett. B **86**, 146 (1979); C.J. Horowitz, D.P. Murdock and B.D. Serot in “Computational Nuclear Physics”, ed. K. Langanke, J.A. Maruhn and S.E. Koonin (Springer, Berlin, 1991); B.D. Serot and J.D. Walecka, Adv. Nucl. Phys. **16**, 1 (1986).
- [44] E.D. Cooper, S. Hama, B.C. Clark and R.L. Mercer, Phys. Rev. C **47**, 297 (1993).
- [45] H. Überall, in “Electron Scattering from Complex Nuclei”, Academic Press, N.Y., (1971).
- [46] J. Engel, E. Kolbe, K. Langanke and P. Vogel, Phys. Rev. C **54**, 2740 (1996).
- [47] C. Giusti and F. D. Pacati, Nucl. Phys. A **473**, 717 (1987).
- [48] K. S. Kim, L. E. Wright and D. A. Resler, Phys. Rev. C **64**, 044607 (2001).
- [49] V. Bernard, L. Elouadrhiri and U. G. Meissner, J. Phys. G **28**, R1 (2002).

TABLES

TABLE I. Integrated cross section, eq. (6), for the quasielastic scattering of ν_μ on ^{12}C , described within the IA and averaged over the LSND muon neutrino spectrum [18], compared with the experimental results for the process $^{12}C(\nu_\mu, \mu^-)X$. Coulomb distortion effects for the outgoing muon are not included and are discussed in the text. In the RFG model the values $k_F = 225$ MeV and (when included) $e_B = 20$ MeV have been used.

Model	$\langle\sigma\rangle$ in 10^{-40} cm^2
RFG	30.8
RFG with e_B	15.8
RSM (PWIA)	20.5
RSM + RMF	16.8
RSM + real ROP	15.1
Expt. value 1995 [18]	$8.3 \pm 0.7 \pm 1.6$
Expt. value 1997 [19]	$11.2 \pm 0.3 \pm 1.8$
Expt. value 2002 [20]	$10.6 \pm 0.3 \pm 1.8$

FIGURES

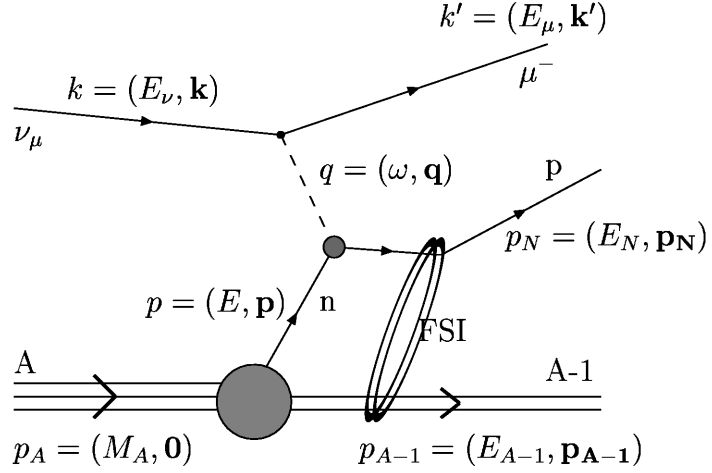


FIG. 1. Born approximation diagram for CC ν -nucleus quasielastic scattering. The impulse approximation is assumed in the hadronic vertex and the possibility of final state interactions between the outgoing nucleon and the residual nuclear system is explicitly shown. The initial nucleon, interacting with the incident neutrino, is in general off mass shell, while for the emitted nucleon the relation $E_N = \sqrt{\mathbf{p}_N^2 + m_N^2}$ holds.

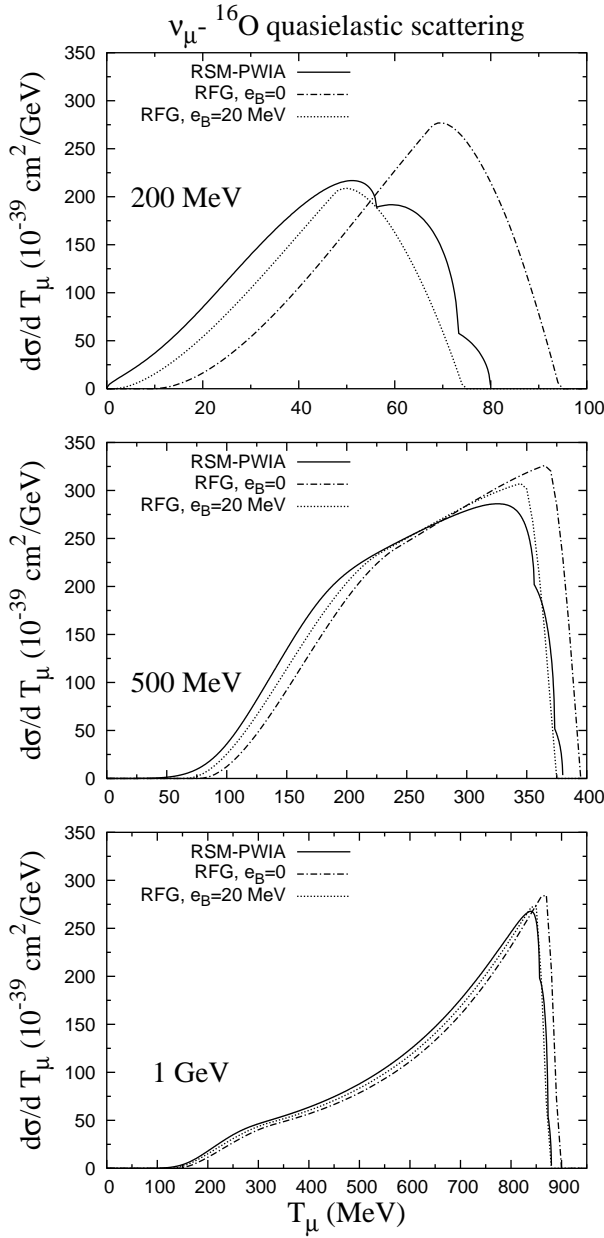


FIG. 2. Differential cross section ($d\sigma/dT_\mu$) versus the outgoing muon kinetic energy, for the quasielastic scattering of muon neutrinos on ^{16}O and for three choices of the incident neutrino energy, as indicated in the panels. The solid curves correspond to the RSM with no final state interaction, while the remaining curves are calculated within the RFG, with $k_F = 225$ MeV and $e_B = 0$ (dot-dashed) and $e_B = 20$ MeV (dotted).

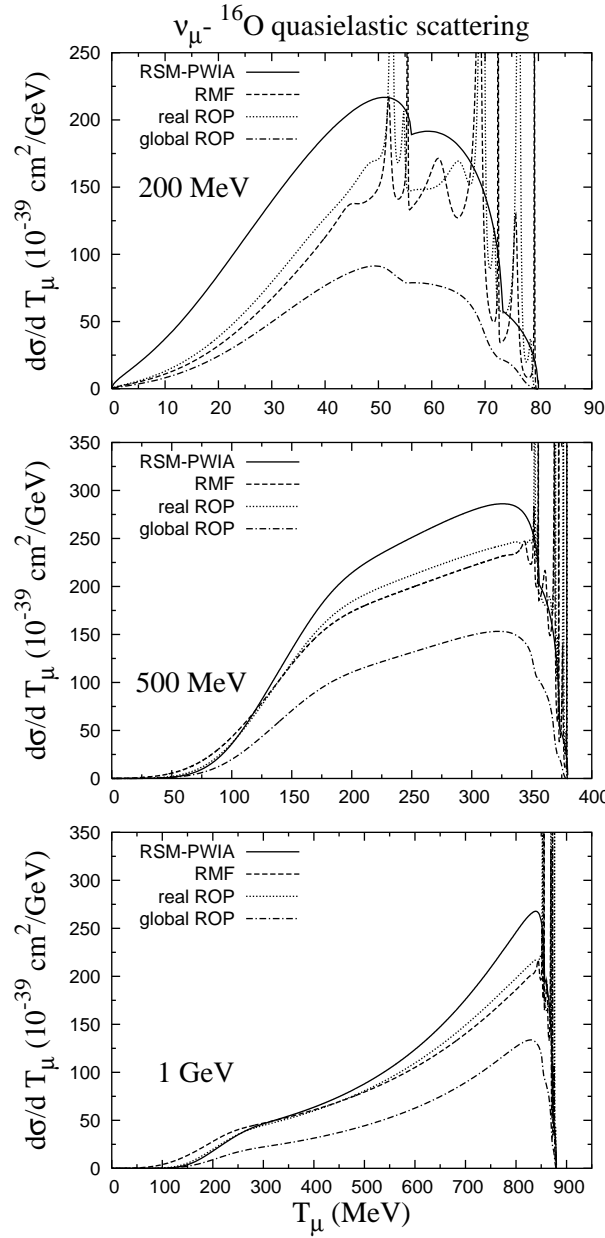


FIG. 3. Same as fig.2, but including FSI effects. All curves are calculated within the RSM model in PWIA (solid), and within the RMF (dashed) and real ROP (dotted) approaches. The RSM result using the global (real and imaginary parts) ROP is also shown (dot-dashed line).

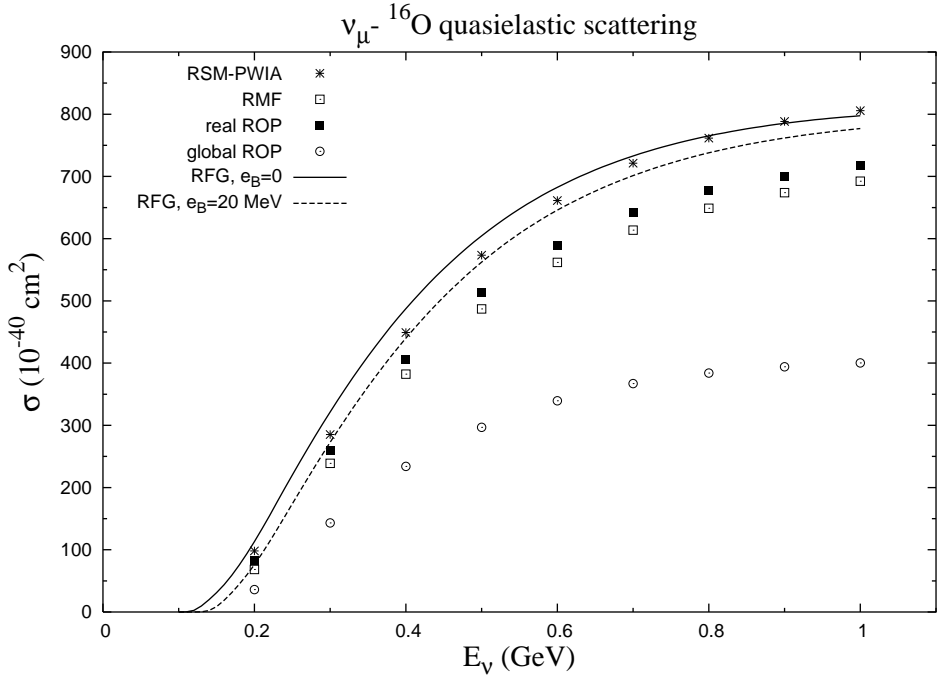


FIG. 4. Integrated cross section $\sigma(E_{\nu})$ for the quasielastic scattering of muon neutrinos on ${}^{16}\text{O}$ as a function of the incident neutrino energy. The curves are calculated within the RFG model with $k_F = 225$ MeV and binding energy $e_B = 0$ (solid line) and $e_B = 20$ MeV (dashed). The points correspond to RSM calculations without FSI (stars) and with FSI effects taken into account within the RMF (empty squares), real ROP (full squares) and global ROP (circles) approaches.

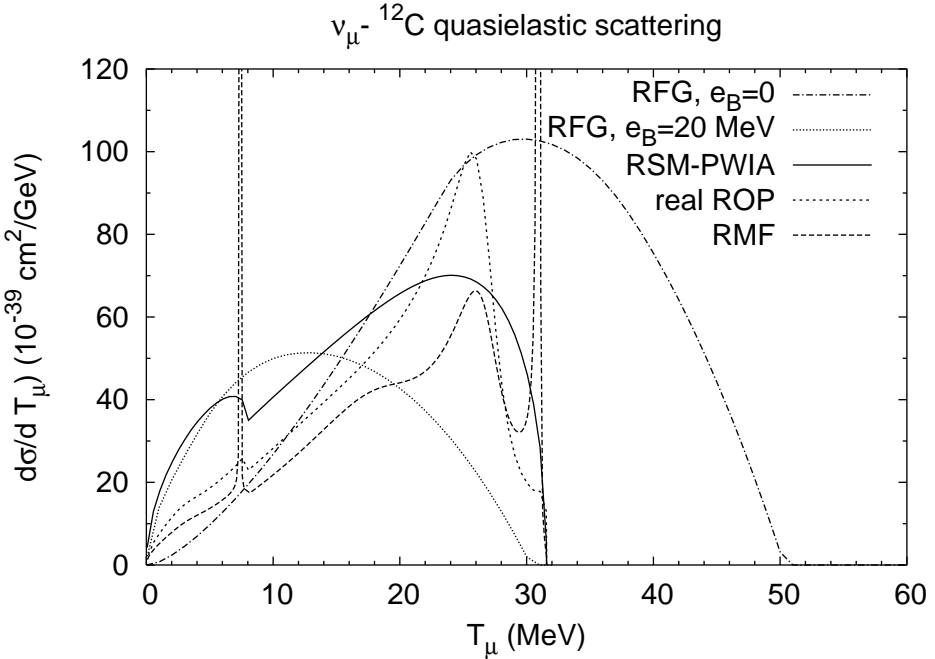


FIG. 5. Differential cross section ($d\sigma/dT_\mu$) versus the kinetic energy transfer T_μ for $\nu_\mu - {}^{12}C$ quasielastic scattering, at $E_\nu = 156$ MeV. The following models have been used: RFG with $k_F = 225$ MeV and binding energy $e_B = 0$ (dot-dashed line) and $e_B = 20$ MeV (dotted), RSM in PWIA (solid) and including FSI effects within the real ROP (short dashed) and the RMF (dashed) approaches.

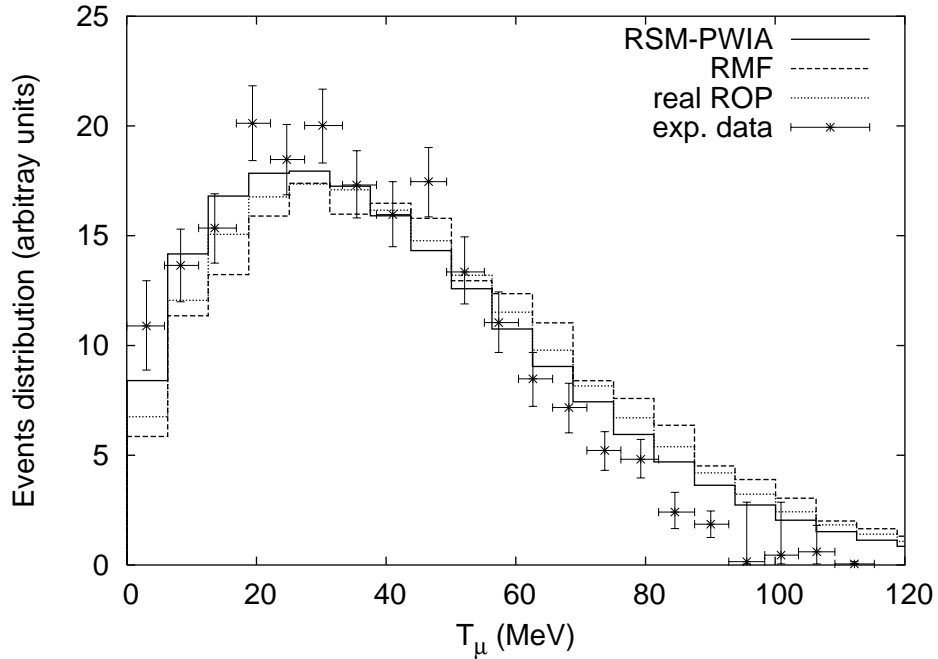


FIG. 6. Observed distribution of muon kinetic energies T_μ compared with the flux-averaged predictions of our RSM, in PWIA (solid line) and including FSI within the RMF (dashed) and purely real ROP (dotted) frameworks. The theoretical distributions have been normalized to the data.